J. Fluid Mech. (1980), *vol.* 97, *part* 4, *pp.* 673–699
Printed in Great Britain

Measurements of heat transfer to a flat plate in a dissociated high-enthalpy laminar air flow

By R. A. EAST

Department of Aeronautics & Astronautics, University of Southampton, U.K.

R. J. STALKER

Department of Mechanical Engineering,† University of Queensland, Brisbane, Australia

AND J. P. BAIRD

Department of Physics, School of General Studies,
Australian National University, Canberra, Australia

(Received 26 May 1979)

Heat-transfer rates from a non-equilibrium hypersonic air flow to flat plates at zero and 12° incidence have been measured in a free piston shock tunnel at stagnation enthalpy levels up to 51 MJ kg^{-1}. Nozzle flow conditions resulted in test section velocities up to 8·1 km s^{-1} and in an experimental regime in which the free stream was chemically frozen and the flat-plate boundary layer was laminar. Estimates of the gas-phase and surface-reaction Damkohler numbers have been made and the heat-transfer results are discussed in this context. At the highest test-section densities non-equilibrium endothermic gas phase reactions involving oxygen atoms in the boundary layer are suggested as a possible mechanism for the observed low heat-transfer rates.

1. Introduction

Heat transfer from non-equilibrium hypersonic flow of high temperature chemically reacting air has been shown to be of importance in determining the aerodynamic heating to which re-entry vehicles of the space-shuttle type are subjected; see for example the work of Rosner (1963), Lordi, Vidal & Johnson (1971) and Bray (1970). Non-equilibrium stagnation point heat transfer has been studied extensively both theoretically and experimentally but relatively few studies exist of flat-plate heat transfer. It is the purpose of the present work to present results of an experimental study of the heat transfer to a flat plate through a non-equilibrium laminar boundary layer in air at Mach numbers in the range 7 to 10 and with free stream stagnation enthalpies and flow velocities up to 51 MJ kg^{-1} and 8·1 km s^{-1} respectively.

The reported experiments, which were performed in the Australian National University 'T3' free piston shock tunnel, do not aim to simulate a particular flight condition since they were performed under conditions of chemically frozen nozzle flow. They are non-simulation experiments and were designed to explore the physical

† Previously at the Department of Physics, School of General Studies, Australia National University, Canberra.

0022–1120/80/4415–8680 $02.00

phenomena associated with non-equilibrium heat transfer at values of stagnation enthalpy, Reynolds number and Mach number relevant to flight in the atmosphere, and as a test of theoretical prediction methods.

For the flat-plate laminar boundary layer studied, the free stream at the boundary-layer edge consisted of a mixture of both atomic and molecular oxygen and nitrogen, even though the free-stream translational temperature was sufficiently low that equilibrium real-gas effects would have been small. At the highest enthalpies, up to 35% of the stagnation enthalpy was frozen as chemical enthalpy of the atomic oxygen and nitrogen. The criteria which determine whether the frozen free-stream chemical enthalpy is recovered, thereby increasing the surface heat transfer rate, are the gas phase and surface reaction Damkohler numbers. These criteria, which control the departure from equilibrium of gas-phase reactions within the boundary layer and of surface reactions at the wall, are considered from the point of view of the reported experimental results. In most conditions, gas-phase recombination within the boundary layer was frozen and the extent to which the surface heat transfer is affected by surface recombination is dependent on the surface material and whether, or not, it is catalytic. The reported experiments aimed to determine the extent, if any, of the contribution to the heat transfer caused by catalytic surface effects.

2. Apparatus

A free piston reflected shock tunnel, the design and operation of which has been described by Stalker (1972) was used to provide the high enthalpy test gas for the heat-transfer experiments. Much higher enthalpies than obtained in conventional reflected shock tunnels are achieved as a consequence of preheating of the driver gas (usually helium) by means of a free piston driven by compressed air.

For the reported tests stagnation enthalpies from 2·0 MJ kg^{-1} to 51 MJ kg^{-1} gave nozzle flow conditions ranging from perfect gas behaviour to a free stream in which oxygen was fully dissociated and a significant mole fraction of atomic nitrogen existed. A range of stagnation pressures from 54 to 430 bar was used. The test medium for the reported experiments was air drawn from the laboratory into a previously evacuated shock tube. A summary of the principal test conditions is given in tables 1 and 2.

Two nozzles were used to expand the heated test gas to hypersonic Mach numbers. A 15° total angle conical nozzle with an exit diameter of 0·305 m and interchangeable throats of diameter 0·635 cm and 1·27 cm provided test-section Mach numbers in the range 7·3 to 10 depending on the stagnation enthalpy level and the stagnation pressure. Higher test-section densities and a Mach number of 5 were obtained by using a contoured nozzle with a throat diameter of 2·54 cm.

Surface heat-transfer measurements were made using two models:

(*a*) 0° incidence flat plate 0·456 m long – plate *A*;

(*b*) 12° incidence flat plate 0·185 m long – plate *B*.

Both models had sharp leading edges ($< 0{\cdot}05$ mm) and the layout of the plates, together with the positions of the heat transfer sensors, is shown in figures 1 and 2. Plate *A* was manufactured from aluminium and its planform was chosen to be within the inviscid nozzle core. Undersurface side walls were fitted in the nominal source

Run type	Time at which $\dot{q}_w$ measured t (μs) see figure 3	h_0 (MJ kg ^{1}) Stagnation enthalpy error $\pm$ 10 %	p_0 (bar) Stagnation pressure error $\pm$ 5 %	M_∞	Test section density $\rho_\infty \times 10^3$ (kg m^{-3})	Test section velocity u_∞ (km s^{-1})	Test section temperature T_∞ (K)	α_0	α_N	γ_f	SR_x^i (theory) equation (12)
A^+	450	51	260	8·3	0·96	8·1	1370	1·0	0·53	1·57	0·327
A	600	38·2	250	7·3	1·18	7·3	1580	1·0	0·33	1·51	0·313
B	730	21·9	270	8·5	2·18	5·74	1150	0·97	0·01	1·45	0·313
C	720	17·0	60	9·1	0·64	5·00	760	0·91	0	1·44	0·318
D	1100	14·2	250	9·2	3·36	4·40	600	0·65	0	1·43	0·326
E	1100	8·7	190	8·6	2·78	4·09	530	0·08	0	1·41	0·327
F	1500	3·08	54	10·0	3·9	2·14	114	0	0	1·40	0·341
G	1500	2·79	170	10·0	12·0	2·06	117	0	0	1·40	0·349
H	1500	2·0	115	10·0	12·0	1·78	79	0	0	1·40	0·364
				(*a*) Conical nozzle – throat diameter 1·27 cm							
B_c	650	16·6	220	5·35	12·28	4·93	2050	0·62	0	1·44	0·359
B_c^+	600	17·0	430	5·21	26·32	5·02	2350	0·49	0	1·44	0·364
				(*b*) Contoured nozzle – throat diameter 2·54 cm							

TABLE 1. Flow conditions at the reference station (see figure 7)

Run type	Time at which $\dot{q}_w$ measured t (μs) see figure 3	h_0 (MJ kg) Stagnation enthalpy error ± 10 %	p_0 (bar) Stagnation pressure error ± 5 %	M_2	$\rho_2 \times 10^3$ (kg m^{-3})	u_2 (km s^{-1})	T_2 (K)	$S\,(R_x)^{\frac{1}{2}}$ (theory) equation (12)
A	600	38·2	250	4·7	3·40	7·01	3539	0·357
B	730	21·9	270	5·31	7·13	5·51	2714	0·354
C	720	17·0	60	5·65	2·14	4·8	1816	0·362
H	1500	2·0	115	5·81	66·5	1·71	216	0·376
			(*a*) Nozzle throat diameter 1·27 cm					
A^+	450	51	260		1·02	7·78	3224	0·374
A	600	38·2	250		1·41	7·01	2940	0·345
B	730	21·9	270		2·89	5·51	2314	0·346
C	720	17·0	60		8·86	4·8	1551	0·358
G	1500	2·79	170		13·1	1·98	261	0·360
			(*b*) Nozzle throat diameter 0·635 cm					

TABLE 2. Flow conditions at the reference station for 12° incidence flat plate *B*

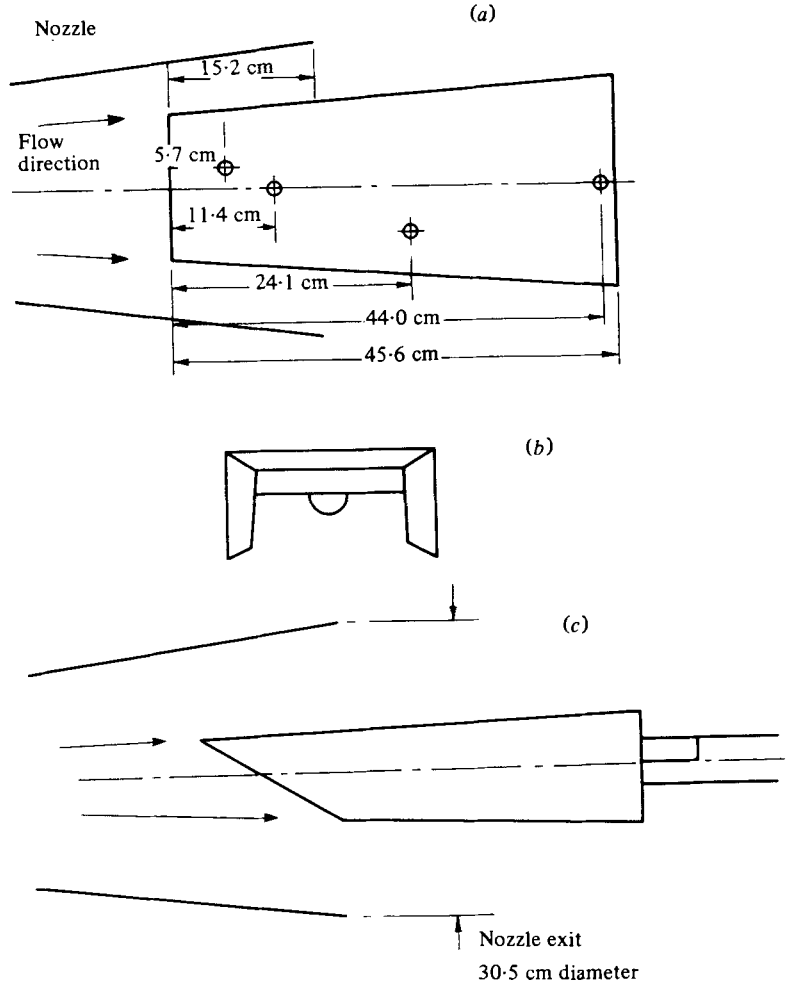

FIGURE 1. Zero incidence flat plate showing position of heat transfer sensors and orientation of plate with respect to the nozzle. (*a*) Plan view of plate A; (*b*) front elevation; (*c*) end elevation.

flow stream direction to prevent undersurface cross flow from affecting the upper surface flow.

Plate *B* was machined from mild steel and incorporated demountable (15·25 × 7·6 cm) inserts on the centre-line as shown in figure 2. Two inserts were manufactured from stainless steel. One was subsequently vacuum coated on its upper surface with a layer of silicon dioxide of approximately 1 μm thickness to act as a non-catalytic surface coating. The leading edges of the inserts were positioned 3·4 cm downstream of the plate leading edge.

The surface heat-transfer measurements were made using vacuum deposited thin-film surface resistance thermometers developed by McCaffrey, East & Stent (1975). Nickel resistance thermometers of nominal thickness 0·05 μm were vacuum evaporated onto the ends of 6 mm diameter quartz rods, the surface of which had been prepared by either optical polishing of flame polishing. Protection from erosion and any electrical conductivity of the test gas was obtained by evaporation of a 0·5 μm protective

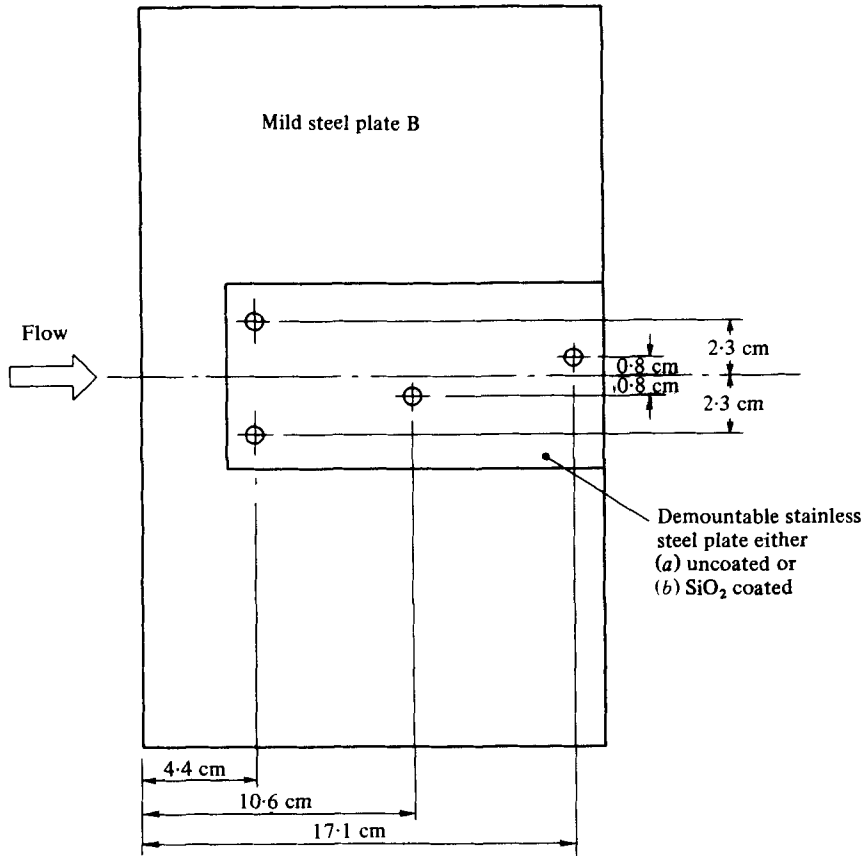

FIGURE 2. Surface of plate B showing gauge positions ~ 12° incidence, plan view.

coating of silicon monoxide which was allowed to oxidize to silicon dioxide. The gauges were mounted in Delrin mounts and inserted flush with the plate surface.

The constant current supply for each of the heat-transfer sensors was obtained using the circuit described by Shultz & Jones (1973). Voltages across the gauges could be set at identical values irrespective of the gauge resistance. The outputs of the resistance thermometers were fed to T-type RC analog circuits, the outputs of which were proportional to the surface heat transfer rate $\dot{q}_w$. The value of $\dot{q}_w$ was obtained from the relationship

$$\dot{q}_w(t) = \frac{2}{(R'C)^{\frac{1}{2}}} \frac{(\rho ck)^{\frac{1}{2}}}{\alpha'} \frac{V(t)-V_0}{V_0}, \tag{1}$$

where V_0 is the initial voltage across the gauge, $V(t)$ is the voltage at time t, ρ is the density of the substrate, c is the specific heat of the substrate, k is the thermal conductivity of the substrate, α' is the temperature coefficient of resistance of the nickel film, and R' and C are the component values of resistance and capacitance used in the analogue network. For the circuit used $R' = 5$ kΩ, $C = 0{\cdot}01$ μF.

Calibrations of the resistance thermometers were made for α' for all gauges by measuring the resistance change when slowly heated in a bath of silicone oil and for $(\rho ck)^{\frac{1}{2}}$ by differential repetitive heating in air and silicone oil using a method described

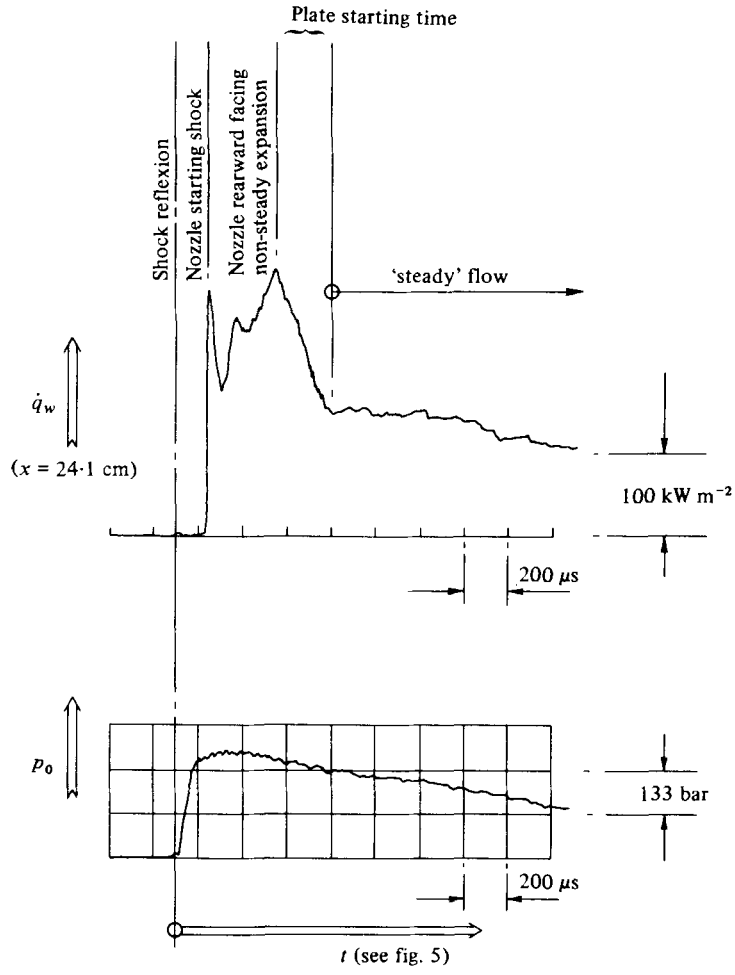

FIGURE 3. Copy of $\dot{q}_w$ and p_0 oscillograms (h_0 = 21·9 MJ kg^{-1}).

by McCaffrey *et al.* (1975). Variations of α' between 0·0008 per °C and 0·0018 per °C were observed for different batches of gauges. The values of $(\rho ck)^{\frac{1}{2}}$ were in agreement with results published by Schultz & Jones (1973) within the limits of accuracy of the calibration method. The value used in the reduction of data was $(\rho ck)^{\frac{1}{2}}$ = 0·151 J cm^{-2} s$^{-\frac{1}{2}}$ for all gauges. The heat-transfer sensor outputs were displayed on Tektronix R561B oscilloscopes and photographed.

3. Surface heat-transfer measurements

Heat-transfer data were obtained for the set of tunnel operating conditions given in tables 1 and 2 for the zero (plate A) and 12° incidence flat plates (plate B). A complete set of data for a given operating condition was obtained from a single tunnel run. A typical oscillogram showing the tunnel stagnation pressure and the surface heat flux is shown in figure 3. The outputs were reduced to heat-transfer rates in kW m^{-2} using equation (1) and typical results are shown in figure 4. The variation of $\dot{q}_w$ in the streamwise direction is compared with the predicted variation of $\dot{q}_w \propto x^{-\frac{1}{2}}$ for a

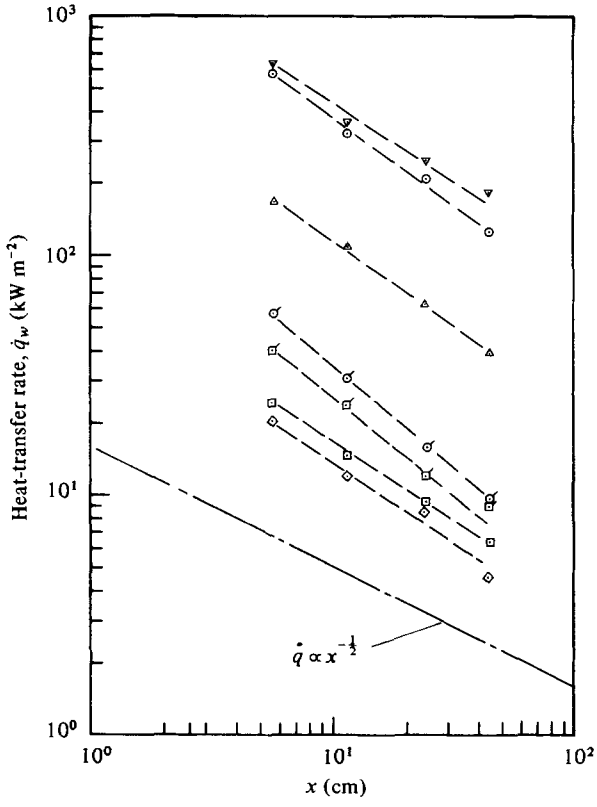

FIGURE 4. Typical flat plate heat transfer data for zero incidence plate A. ▽, Run A^+; ⊙, run B; ⊡, run D; △, run E; □, run F; ⊙, run G; ◇, run H; – – –, mean line through data points. Run types A^+ to H defined in table 1.

laminar boundary layer in figure 4. The experimental values show a stronger inverse dependence on x which is attributed to the conical nozzle source flow effect. It is observed that the experimental range of conditions resulted in values of $\dot{q}_w$ varying by more than two orders of magnitude.

4. Test-section flow characteristics and reduction of data

4.1. *Flow starting time*

The times available for heat-transfer measurements, which are limited by the times required to start the nozzle flow and for boundary-layer establishment and are terminated by the arrival of the helium driver gas, were deduced from the surface heat-transfer rate oscillograms. Figure 3 shows a typical record on which is indicated the forward facing shock and subsequent rearward facing expansion which propagate through the nozzle and form the typical nozzle starting wave system as described by Smith (1966). The arrival of the head of the rearward-facing expansion may be regarded as the termination of the nozzle starting process. However, the process by which the boundary layer reaches a steady state may be considered as similar in many respects to that which occurs on a flat plate in a shock tube after the passage of the incident shock wave. For the nozzle conditions, the rearward-facing expansion is

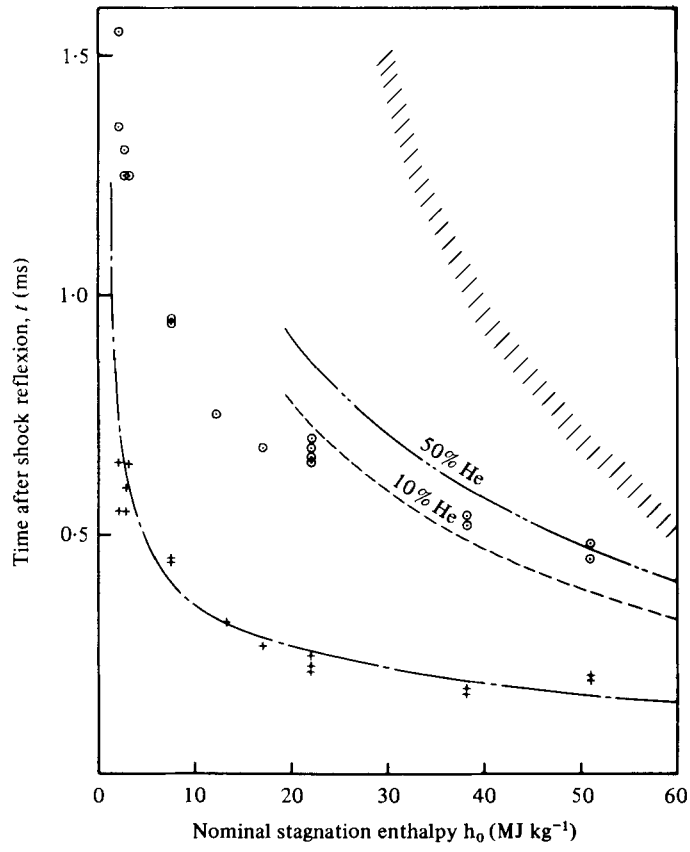

FIGURE 5. Zero incidence flat plate flow starting time. — – —, Plate starting time $t = x/0{\cdot}3u$ (Davies & Bernstein 1969); – – –, 10% helium contamination by number density (Crane 1975); — – – —, 50% helium contamination by number density (Crane 1975); //////////, drainage time estimate. +, experiment, plate starting time; ⊙, experiment, nozzle plus plate starting time.

steep fronted and may be considered as the equivalent of a shock wave. The subsequent transition from a thin non-steady boundary layer with relatively high surface heat flux to a steady boundary layer with a lower steady-state heat flux is similar to that described by Davies & Bernstein (1969) who have suggested an empirical relation for the time t required to reach a steady state given by $t = x/0{\cdot}3u$, where x is the plate length and u is the external flow velocity.

Experimental data shown in figure 5 demonstrate good agreement with the empirical prediction of the plate starting time. Also shown is the total nozzle plus plate starting time, together with estimates of the tunnel running time based on (i) drainage time of the hot gas and (ii) the earlier arrival of helium driver gas as detected by test section mass-spectrometric sampling reported by Crane (1975). The earlier arrival of helium is attributed to the reflected shock bifurcation which occurs on its interaction with the wall boundary layer in the shock tube as suggested by Davies & Wilson (1969). Stalker & Crane (1978) have shown that this effect can be used to predict the observed onset of helium contamination at the high values of shock Mach number appropriate to the high enthalpy conditions.

The evidence from the starting time and mass-spectrometer investigations is summarized in figure 5. This suggests that steady state contamination free heat-transfer measurements should just be possible at stagnation enthalpy levels of 20 MJ kg^{-1} but that some contamination of the test gas with helium will occur before a steady state is established at enthalpies in excess of this value.

4.2. *Test-section flow characteristics*

The reduction of the measured surface heat fluxes to non-dimensional Stanton number S requires a detailed knowledge of the test-section density, velocity and recovery enthalpy. In addition, the test-section temperature is necessary to obtain the viscosity required in the calculation of local Reynolds numbers. The detailed test-section data on which all subsequent data reduction has been based are summarized in tables 1 and 2. These data have been obtained at a reference position 4·5 cm downstream of the nozzle exit and an allowance for nozzle source flow effects at other positions in the flow from the 7·5° semi-angle conical nozzle has been made as described later.

The stagnation enthalpy was calculated from measurements made in the shock tube of shock speed and pressure. Pressure measurements were made using Kistler piezo-electric transducers with a suitable protective covering to minimize thermal influence on the outputs. Shot to shot repeatability over a long period of time resulted in pressure levels repeatable to within $\pm$ 12% of the mean. Calculations of the reflected shock conditions were based on an equilibrium real air model using measured values of the initial shock-tube pressure and temperature. An isentropic expansion (or compression) from the reflected shock pressure to the measured pressure after shock reflexion was assumed in order to calculate the stagnation enthalpy and to account for departures from the tailoring condition.

The test-section velocity was deduced from interferometric measurements behind normal shock waves ahead of circular cylinders and from oblique shocks on wedges. Together with test section measurements of pitot pressure p_t, measurements of the test-section density p_∞ may be used to deduce the free-stream velocity u_∞ using the relationship $u_\infty = (p_t/0{\cdot}90\rho_\infty)^{\frac{1}{2}}$. Measurements were made over a range of stagnation enthalpies and have been compared with non-equilibrium nozzle flow predictions using the method of Lordi, Mates & Moselle (1966). Vibrational non-equilibrium has been included in the prediction method. These results, shown in figure 6, have been reported by Stalker & Stollery (1975). The analysis which results in the test section velocity assumes that the composition of the test gas is air. If contamination by the helium driver gas is assumed, the theoretical predictions of fringe shift at high test-section velocities suggest that ambiguous interpretations of these measurements are possible. Since Crane (1975) has detected the early arrival of helium in the test-section by mass-spectrometer measurements, the test-section velocity measurements should be treated with caution at enthalpies in excess of about 25 MJ kg^{-1}.

A further inaccuracy which could affect the test-section velocity is radiative enthalpy loss from the reservoir gas. Calculations suggest that this is unlikely to be significant for running conditions up to stagnation enthalpies of 40 MJ kg^{-1} at 250 bar.

Direct measurement of the nozzle flow static temperature is difficult and has not been attempted. In order to predict the test-gas viscosity, the static temperature has been predicted using the non-equilibrium nozzle flow program including the effect

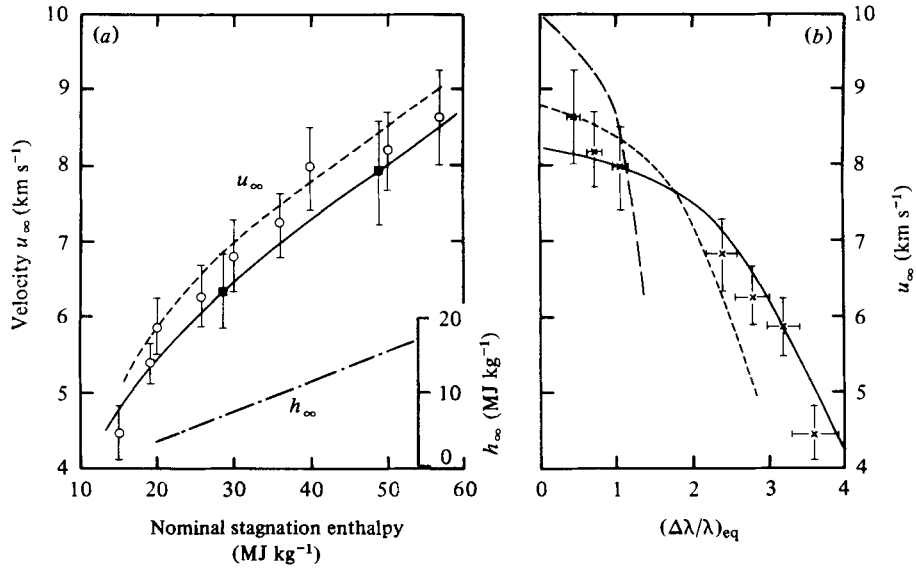

FIGURE 6. Test section flow characteristics, see Stalker & Stollery (1975): (*a*) Velocity and enthalpy; (*b*) normal shock equilibrium fringe shift. ——, theory, 0% helium contamination; – – –, theory, 40% helium contamination; — — —, theory, 80% helium contamination; —·—, test section static enthalpy h_∞. ⊖, Experiment, oblique shocks; ▮, experiment, normal shocks; ⊢⊠⊣, experimental fringe shift.

of vibrational non-equilibrium. Measurements of the oxygen and nitrogen dissociation fraction in the frozen free stream by Stalker & McIntosh (1973) confirm the validity of this method for predicting test section composition and suggest it may be used to estimate the static temperature providing the reservoir conditions are helium free.

The frozen ratio of specific heats may be written as

$$\gamma_f = (7 + 5\tilde{r})/(5 + 3\tilde{r}),$$

where $\tilde{r}$ is the ratio of monatomic to diatomic particles, and is given by

$$\tilde{r} = \frac{2\alpha_O + 8\alpha_N}{5 - (\alpha_O + 4\alpha_N)}$$

in which α_O and α_N are repectively the test section frozen dissociation fractions of oxygen and nitrogen. Values of γ_f have been obtained using this expression with α_O and α_N evaluated using the nozzle flow program.

The test-section Mach number follows directly from the predictions of the test section velocity u_∞, temperature T_∞ and γ_f using the relationship

$$M_\infty = u_\infty/(\gamma_f R_\infty T_\infty)^{\frac{1}{2}}$$

where R_∞ is the gas constant based on the predicted test-section composition.

Calculation of the flow properties external to the boundary layer on the 12° plate have been based on this Mach number and values of γ_f assuming frozen flow downstream of the oblique shock wave formed at the wedge leading edge. The properties are summarized in table 1.

These test flow conditions were obtained at a particular reference station in the nozzle exit. For the 7·5° semi-angle conical nozzle the local flow conditions adjacent

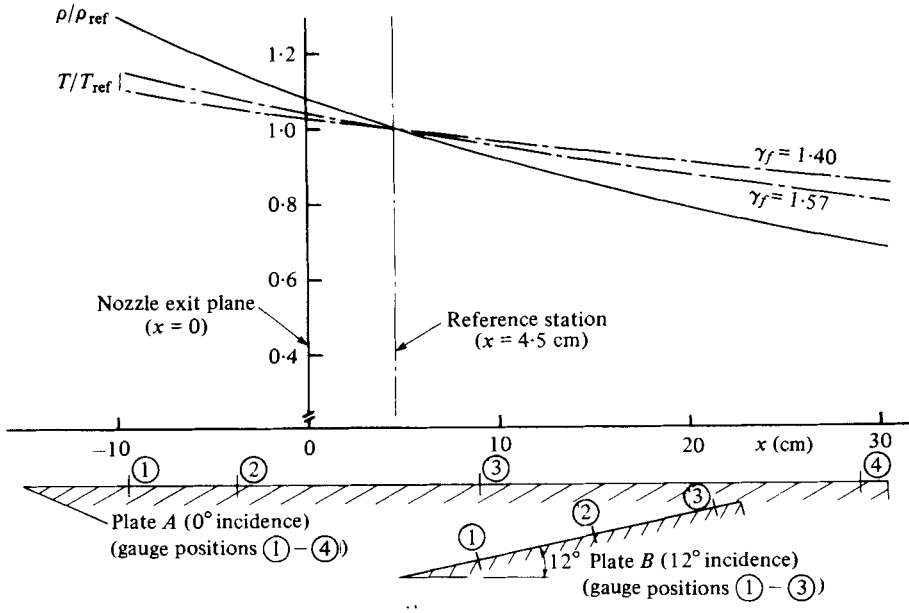

FIGURE 7. Calculated streamwise density and temperature variation along the nozzle axis.

to the positions at which heat transfer was measured were found by assuming that they could be related to the reference conditions by isentropic expansion or compression for downstream or upstream positions respectively. Chemically and vibrationally frozen flow conditions and the high-Mach-number approximation of constant free-stream velocity were assumed. The predicted density and temperature variations are shown in figure 7. The heat-transfer data were reduced to non-dimensional form in terms of the Stanton number S by using these estimated local free-stream conditions. Similarly, Reynolds numbers were based on local free-stream density and viscosity.

For the zero incidence heat-transfer measurements this procedure should adequately account for streamwise temperature and density gradients, but for the 12° incidence case, an additional effect of flow angularity for gauge positions away from the nozzle axis is present. No allowance has been made for this effect.

4.3. *Reduction of the heat-transfer data*

Local values of the Stanton number, S, and Reynolds number R_x were obtained from the following definitions

$$S = \frac{\dot{q}_w}{\rho_e u_e (h_r - h_w)} \tag{1}$$

and

$$R_x = \frac{\rho_e u_e x}{\mu_e}, \tag{2}$$

where the suffix e refers to local conditions at the edge of the boundary layer, suffix w refers to wall conditions and the recovery enthalpy h_r is given by

$$h_r = h_e + \sigma^{\frac{1}{2}}(\tfrac{1}{2}u_e^2) \tag{3}$$

where σ is the Prandtl number.

For equilibrium conditions, the free-stream enthalpy h_e should include the chemical

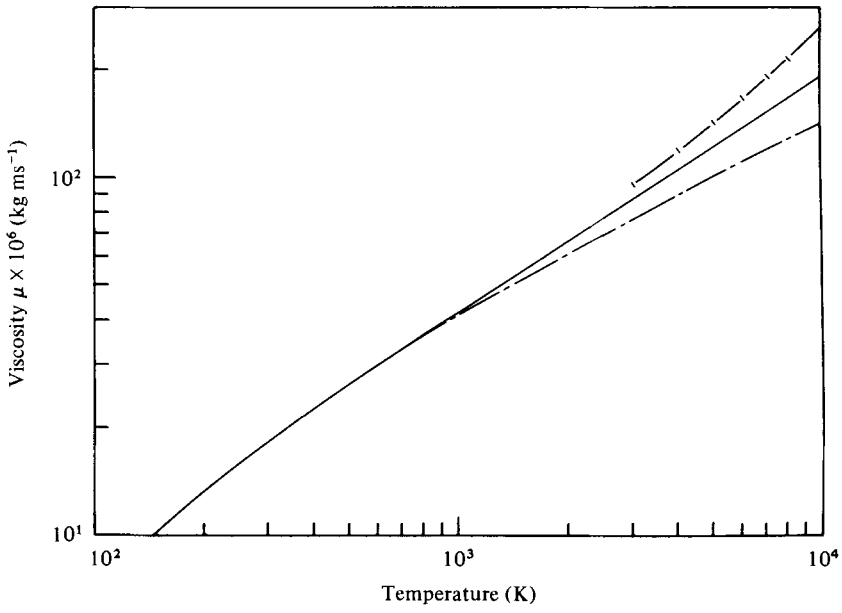

FIGURE 8. Viscosity of air at high temperatures. ——, Lennard–Jones intermolecular potential, Hirschfelder *et al.* (1954, table 8.6-4); — | —, intermolecular potential $\sim A/r^n$ ($n = 6$) Bauer & Zlotnick (1959); — · —, Sutherlands formula $\mu = \beta T^{\frac{3}{2}}(T+S)^{-1}$, $\beta = 1{\cdot}458 \times 10^{-6}$ kg s^{-1} m^{-1} K$^{-\frac{1}{2}}$, $S = 110{\cdot}4$ K.

enthalpy h_{chem}, vibrational enthalpy h_{vib} and the translational and rotational enthalpy $c_{pf}T_e$, whereas, for frozen conditions it includes only $c_{pf}T_e$. Thus, the equilibrium recovery enthalpy $(h_r)_{\text{eq}}$ and the frozen recovery enthalpy $(h_r)_f$ are given by

$$(h_r)_{\text{eq}} = c_{pf}T_e + h_{\text{chem}} + h_{\text{vib}} + \sigma^{*\frac{1}{2}}(\tfrac{1}{2}u_e^2) \tag{4}$$

and

$$(h_r)_f = c_{pf}T_e + \sigma^{*\frac{1}{2}}(\tfrac{1}{2}u_e^2) \tag{5}$$

where c_{pf} is the frozen specific heat at constant pressure and the Prandtl number σ^* is evaluated at intermediate enthalpy conditions.

All of the reported data have been reduced using the assumption of $(h_r)_{\text{eq}}$ in the definitions of Stanton number. Thus departures between theory and experiment will provide some measure of how much of the chemical enthalpy is being recovered either by gas phase combination in the boundary layer and/or by surface recombination.

An important quantity required in the data reduction is the viscosity of the test gas. For the reported experiments the external flow consisted of a frozen mixture of atomic and molecular nitrogen and oxygen depending on the level of stagnation enthalpy. For the intermediate enthalpy prediction method, viscosity data were required at temperatures up to 6300 K. Many authors have considered the transport properties of equilibrium dissociated air (see for example Bauer & Zlotnick 1959) but little information exists for compositions typical of those found in chemically frozen nozzle flows. However, Dorrance (1962) shows that the presence of atomic species in an ideal dissociating gas has only a small effect on the viscosity. Thus, the values of viscosity of air at high temperatures have been taken for an equilibrium

mixture and the data given by Hirschfelder, Curtis & Bird (1954), calculated using the Lennard–Jones intermolecular potential model, were used. These data are summarized in figure 8, and compared to the simple relationship of Sutherland's formula and with Bauer & Zlotnick's prediction based on an intermolecular potential of the form Ar^{-n}, where r is the intermolecular distance and $n = 6$. It is recognized that the use of this data cannot be rigorously substantiated under the experimental conditions studied but it is unlikely to be in error by more than 10% at temperatures up to 2000 K which covers the range of external flow temperatures for the zero incidence plate. However, the use is more conjectural at the higher free-stream temperatures on the 12° incidence plate.

4.4. *Accuracy of the data*

The reported experiments have been carried out under flow conditions which are extreme for shock tunnel facilities and obtainable only by using the unique free piston driver gas compression mode exploited in the facility. A number of sources of experimental error and uncertainty arise.

The experimental error associated with the measured surface heat-transfer rate is assessed to be $\pm 5\%$ taking into account gauge and recording instrument calibration factors only.

Measurements of stagnation enthalpy, obtained from shock-speed measurements have an estimated accuracy of $\pm 10\%$. Pressure measurements have an estimated accuracy of $\pm 5\%$.

Additional errors are evident in the values of S and R_x owing to uncertainties in the free-stream properties ρ, u and μ. These are based on non-equilibrium nozzle flow calculations and measured values of pitot pressure in the nozzle, as described earlier. The value of μ, the free-stream viscosity is also a source of error. The free stream is known to consist of a non-equilibrium mixture of atoms and molecules, whereas the values of μ used in the reduction of data were taken for an equilibrium mixture at the predicted free-stream conditions.

Quantification of the accuracy of the $R_x - S$ data, which is dependent on all these factors, is difficult but, it is estimated that the largest errors which occur at the highest enthalpy conditions are likely to be less than $\pm 20\%$ for S and $\pm 10\%$ for R_x.

5. Prediction of the surface heat-transfer rates including surface catalysis effects

For the highest enthalpy experiments the nozzle freezing phenomenon results in a free stream at the edge of the boundary layer in which significant concentrations of atomic oxygen and nitrogen are present. The surface heat-transfer rate $\dot{q}_w$ is dependent on the recombination of the atomic species, whether by gas phase reactions within the boundary layer, or by surface reactions in which the catalytic effect of the particular surface plays the dominant role when the gas phase reactions are frozen. The lowest surface heat-transfer rate results when both the gas phase and surface reactions remain frozen (non-catalytic surface). The magnitude of the fractional reduction from the equilibrium heat transfer is equal to $h_{\text{chem}}/(h_r - h_w)$, where h_{chem} is the chemical enthalpy which would result from recombination of all the atomic species present at the boundary-layer edge. Nozzle flow calculations for the

highest enthalpy condition studied (51 MJ kg^{-1}) show that the free stream consists of a frozen mixture of almost fully-dissociated oxygen together with atomic and molecular nitrogen for which the fraction $h_{\text{chem}}/(h_r - h_w)$ is approximately 0·35. Proportionate reductions in heat transfer rate between fully catalytic and non-catalytic surfaces should be evident for flow conditions which result in frozen gas phase boundary-layer reactions.

The criterion determining whether the boundary layer remains frozen is the gas phase Damkohler number. This compares the characteristic boundary-layer particle diffusion time τ_d with a characteristic reaction time τ_r. Chung (1965) has shown that for a flat-plate laminar boundary layer the gas phase Damkohler number ζ_g is given by

$$\zeta_g = \frac{4x}{u_e} \frac{k_{R_0}}{T_e^{\omega+2}} \left(\frac{p}{R_0}\right)^2 = \frac{\tau_d}{\tau_r}, \tag{6}$$

where $k_{R_0} = 2k_R T^\omega$ in which k_R is the specific recombination rate coeffiicent, ω is the exponent of temperature in the expression for $k_R = A/T^\omega$, R_0 is the universal gas constant and p, T_e and u_e are respectively the static pressure, temperature and velocity at the edge of the boundary layer distant x from the plate leading edge.

Values of ζ_g have been calculated for the reactions

$$\mathrm{O} + \mathrm{O} + \mathrm{M} \rightarrow \mathrm{O}_2 + \mathrm{M}, \quad \text{where} \quad \mathrm{M} = \mathrm{O}$$

for which $2k_R = 2{\cdot}25 \times 10^{20} T^{-\frac{3}{2}}$ cm^6 g^{-1} mole^{-2} s^{-1} and

$$\mathrm{N} + \mathrm{N} + \mathrm{M} \rightarrow \mathrm{N}_2 + \mathrm{M}, \quad \text{where} \quad \mathrm{M} = \mathrm{N}$$

for which $2k_R = 2{\cdot}36 \times 10^{21}$ cm^6 g^{-1} mole^{-2} s^{-1}. These are tabulated for the various tunnel operating conditions in table 3. The values of ζ_g for the oxygen atom recombination are of order 10^{-2} or less for all conditions apart from conditions D and E. The calculations suggest frozen boundary layer behaviour for atomic oxygen recombination for conditions A^+, A, B and C with the possibility of approach to equilibrium for condition D and more so for condition E. For the more rapid nitrogen atom recombination, the values of ζ_g are an order of magnitude greater than for ζ_g for oxygen recombination, but for the running conditions for which nitrogen atom recombination would be expected to be significant (A^+ and A) the values of ζ_g are approximately 4×10^{-2} suggesting that the boundary layer remains effectively frozen.

If ζ_g is sufficiently small, atom species will not recombine in the boundary layer and will diffuse to the surface. The extent of surface recombination is determined by the catalytic nature of the surface material and is characterized by a surface Damkohler number ζ_s. This gives the ratio of the characteristic particle diffusion time to the characteristic time for surface reaction. Chung (1965) defines ζ_s for a flat plate laminar boundary layer as follows:

$$\zeta_s = \frac{\sigma \rho_w k_w x^{\frac{1}{2}}}{L(\frac{1}{2}\rho_e u_e \mu_e l)^{\frac{1}{2}}} = \frac{\tau_d}{\tau_w} \tag{7}$$

where σ is the Prandtl number, L is the Lewis number given by $\rho D c_p/k$ (where D is the diffusivity, k the thermal conductivity and c_p the specific heat at constant pressure), k_w is the specific wall reaction rate given by

$$k_w = \gamma' \left(\frac{R_0 T}{2\pi M_A}\right)^{\frac{1}{2}},$$

Run type (see table 1)	0° incidence (x = 45·6 cm) (1·27 cm diameter throat) conical nozzle		12° incidence (x = 18·5 cm) (1·27 cm diameter throat) conical nozzle		12° incidence (x = 18·5 cm) (0·635 cm diameter throat) conical nozzle		0° incidence (x = 4·56 cm) (2·54 cm diameter throat) contoured nozzle	
	ζ_g	$E(x, \sigma)$	ζ_g	$E(x, \sigma)$	ζ_g	$E(x, \sigma)$	ζ_g	$E(x, \sigma)$
A^+	$2{\cdot}49 \times 10^{-3}$	5·12	—	—	$0{\cdot}745 \times 10^{-3}$	4·95	—	—
A	$3{\cdot}26 \times 10^{-3}$	3·31	$8{\cdot}41 \times 10^{-3}$	2·25	$1{\cdot}40 \times 10^{-3}$	3·85	—	—
B	$9{\cdot}46 \times 10^{-3}$	2·80	$2{\cdot}90 \times 10^{-2}$	1·59	$4{\cdot}46 \times 10^{-3}$	2·74	—	—
C	$1{\cdot}8 \times 10^{-3}$	5·12	$8{\cdot}09 \times 10^{-3}$	3·86	$1{\cdot}47 \times 10^{-3}$	6·16	—	—
D	$3{\cdot}45 \times 10^{-3}$	2·92	—	—	—	—	—	—
B_c	—	—	—	—	—	—	$1{\cdot}93 \times 10^{-1}$	0·68
B_c^+	—	—	—	—	—	—	$6{\cdot}87 \times 10^{-1}$	0·44

ζ_g ~ Gas phase Damkohler number for O atom recombination.

$E(\sigma, x)$ ~ Parameter defined by equation (9); related to surface reaction Damkohler number for O atom surface recombination (assumed $k_w = 50$ cm s^{-1}).

TABLE 3. Gas phase and surface reaction Damkohler numbers

l is the ratio of the density–viscosity product $\rho\mu/\rho_e\mu_e$, and suffices w and e refer to wall and boundary-layer edge conditions respectively. γ' is the surface catalytic efficiency and M_A is the molecular weight of the atomic species.

For small values of ζ_s the diffusion rate is much greater than the wall reaction rate and the phenomenon will be surface reaction limited. In this limit the surface reaction is 'frozen' and all surfaces are effectively non-catalytic. The concentration of atomic species at the wall will be identical to the free-stream value at the edge of the boundary layer for $\zeta_s \to 0$. No recombination occurs at the wall and lowest surface heating rate will be evident in this limit, provided that the gas phase reactions remain frozen.

For large values of ζ_s, the surface reaction rate is much greater than the diffusion rate and virtually all of the atomic species arriving at the wall will be recombined, thus increasing the surface heating rate. This limit is the diffusion limited regime. Glassy materials such as pyrex or quartz have values of γ' of order 10^{-4}, whereas metallic surfaces generally have values up to 10^{-1}. An experimental situation may therefore exist for which the values of ζ_s for the different materials may differ by three orders of magnitude and in which almost all of the chemical enthalpy difference may be evident in the measured surface heat transfer rate.

Vidal & Golian (1967) have reported an extension of Crocco's compressible laminar boundary-layer solution to include species diffusion for zero pressure gradient and with $\mu \propto T^a$, where a is a constant. The result for the dimensionless heat transfer rate S', is

$$S' = \frac{C_f}{2\sigma^{\frac{2}{3}}}\left\{1 + (\sigma^{\frac{1}{2}} - 1)\left[\frac{u_e^2}{2(h_0 - h_w)}\right] - \left[\frac{\alpha_e h_D}{h_0 - h_w}\right]\frac{\alpha_w}{\alpha_e}\right\}, \tag{8}$$

where $S' = \dot{q}_w/\rho_e\mu_e(h_0 - h_w)$, $\alpha_w/\alpha_e = E(x,\sigma)/[1 + E(x,\sigma)]$, h_D is the chemical enthalpy associated with the dissociated species, h_0 is the stagnation enthalpy, α is the dissociation fraction, σ is the Prandtl number, and $E(x,\sigma)$ is directly related to the surface Damkohler number as follows

$$E(x,\sigma) = \frac{C_f}{2\sigma^{\frac{2}{3}}}\left[\frac{\rho_e\mu_e}{\rho_w k_w}\right] = \frac{0{\cdot}664}{\sqrt{2}}\frac{\sigma^{\frac{1}{3}}}{L}\frac{1}{\zeta_s}, \tag{9}$$

since

$$C_f R_x^{\frac{1}{2}} = 0{\cdot}664\left(\frac{\rho\mu}{\rho_e\mu_e}\right)^{\frac{1}{2}}$$

In the non-catalytic wall limit, $E \to \infty$ and $\alpha_w/\alpha_e = 1$ which, for $\sigma = 1$, reduces the Stanton number S' by the fraction

$$\frac{\alpha_e h_D}{h_0 - h_w}.$$

At high enthalpies, intermediate enthalpy concepts have been used to predict surface heat-transfer rates. Hayes & Probstein (1959) following Eckert, introduce an intermediate enthalpy h^* given by

$$h^* = 0{\cdot}5(h_e + h_w) + 0{\cdot}22(h_r - h_e)$$

where the recovery enthalpy h_r is

$$h_r = h_e + \tfrac{1}{2}\sigma^{*\frac{1}{2}}u_e^2.$$

In this method the variation in the density–viscosity product across the boundary layer is accounted for in the expression for skin friction C_f where

$$C_f R_x^{\frac{1}{2}} = 0{\cdot}664\left(\frac{\rho^*\mu^*}{\rho_e\mu_e}\right)^{\frac{1}{2}}$$

with $R_x = \rho_e u_e x/\mu_e$. With the Stanton number defined in terms of the recovery enthalpy h_r as

$$S = \dot{q}_w/\rho_e u_e(h_r - h_w) \tag{10}$$

the Reynolds analogy gives

$$S = \tfrac{1}{2}C_f(\sigma^*)^{-\frac{2}{3}} \tag{11}$$

and

$$SR_x^{\frac{1}{2}} = 0{\cdot}332(\sigma^*)^{-\frac{2}{3}}\left(\frac{\rho^*\mu^*}{\rho_e\mu_e}\right)^{\frac{1}{2}}. \tag{12}$$

Allowing for the different definitions of S and S', this result is seen to be similar to that of Vidal & Golian (1967) [equation (8)] for the case when $\alpha_w/\alpha_e \to 0$ (fully catalytic surface limit) except that the Prandtl number, σ, and the density–viscosity product are more realistically evaluated at conditions appropriate to the intermediate enthalpy.

Generalizing the intermediate enthalpy result for the frozen flow limit $\alpha_w/\alpha_e = 1$ gives the following result for the Stanton number S_f appropriate to the frozen limit

$$S_f = \frac{C_f}{2}(\sigma^*)^{-\frac{2}{3}}\left\{1 - \frac{h_{\text{chem}}}{h_r - h_w}\right\} \tag{13}$$

where $h_{\text{chem}}/h_r - h_w$ represents the fraction of the recovery enthalpy associated with frozen chemistry.

For surface conditions intermediate between those for frozen and equilibrium surface reactions, the Stanton number should be evaluated from equation (8) with the appropriate value of $E(x, \sigma)$ calculated for the particular case.

To establish bounds for the currently reported experimental conditions, values of $E(x, \sigma)$ have been calculated for the trailing edge position of both the 0° and 12° plates using equation (8). These have been based on a wall recombination rate $k_w = 50$ cm s^{-1} which might be considered typical for O and N atom recombination on oxidized metallic surfaces at $T_w = 300$ K. From table 3 it is observed that $1{\cdot}59 < E(x, \sigma) < 5{\cdot}12$ for the conical nozzle experiments, indicating that the chemical enthalpy fraction which would be recovered at the wall would be in the range 0·39 to 0·16. Lower values of $E(x, \sigma)$ are noted for the contoured nozzle conditions but it is possible that these experiments are further complicated by endothermic gas phase boundary-layer reactions as discussed later.

For surface conditions appropriate to glassy materials, the corresponding wall recombination rate k_w is of the order 1 cm s^{-1} and the chemical enthalpy fractions recovered would be in the range 0·013 to 0·003.

In summary, therefore, the values of $E(x, \sigma)$ for the conical nozzle experiments given in table 3 suggest that the amount of the frozen free-stream chemical enthalpy which could be recovered at the wall and would be evident in surface heat-transfer measurements will be small under all the experimental conditions explored. Possible exceptions are the extreme trailing-edge position of the 12° plate, particularly for the higher Reynolds numbers associated with the 1·27 cm diameter throat experiments. However, since the frozen free-stream chemical enthalpy is only about 20% of the recovery enthalpy $(h_r)_{\text{eq}}$, differences of less than 6% in the absolute magnitudes of measured values of $\dot{q}_w$ for different plate surface conditions would require to be resolved to detect the departure from the frozen surface-reaction limit. Such differences are not detectable within the current repeatability of tunnel operating conditions and

the knowledge of the free-stream conditions from run to run. It is expected from theoretical considerations, therefore, that the achievable experimental conditions will result in $\dot{q}_w$ measurements close to the frozen limit.

6. Boundary-layer chemical reactions

The calculations described earlier (with the possible exception of 2·54 nozzle throat experiments) show that for all of the conditions of the experiments direct gas phase recombination of the frozen free-stream oxygen and nitrogen atoms is most improbable since all values of the gas phase Damkohler number are less than 10^{-2}. The possibility exists, however, of endothermic chemical reaction involving oxygen atoms taking place, of which the following are considered:

(1) $N_2 + O \rightarrow NO + N$;
(2) $NO + O \rightarrow O_2 + N$;
(3) $O_2 + O \rightarrow O + O + O$.

At the conditions prevailing in the plate boundary layer (high concentrations of N_2 and O, and temperatures in the range 2000 K–4000 K) the forward reaction of (1) is the dominant process of these three. Reactions (2) and (3) are less significant and the reverse reactions can generally be ignored, in the case of (2) because high concentrations of O_2 and N are not experienced simultaneously in the boundary layer, and in the case of (3), as a consequence of low densities. Only for the higher density experiments (see table 1) is there a likelihood of O atom recombination. The forward endothermic reactions of (1), (2) and (3) provide a possible mechanism for further reductions in the surface heat transfer below the non-catalytic surface result shown in figures 12 and 13, providing surface recombination of the species formed in these reactions does not take place.

An estimate of the magnitude of possible boundary-layer reaction effects has been made using a simple boundary-layer model and integrating the equation for the energy ϵ absorbed by the reactions per unit mass along a streamline.

The enthalpy distribution h across the boundary layer was assumed to be similar to that for a non-reacting boundary layer with unit Prandtl number and Lewis number. Thus

$$h = h_w + (H_e - h_w)\, u/u_e - \tfrac{1}{2}u^2, \tag{14}$$

where u is the local velocity, u_e is the free-stream velocity, H_e is the free-stream stagnation enthalpy ($= h_e + \frac{1}{2}u_e^2$) and h_w is the enthalpy at the wall.

The assumptions of this equation imply (1) that the diffusion of reactants across stream-tubes does not have a significant effect on the concentrations and (2) that the change in thermal energy transport caused by changes in temperature gradients resulting from reactions is small in comparison with conduction across stream-tubes in the absence of reactions. The energy rate of absorption per unit mass along a streamline is given by

$$u\frac{d\epsilon}{dx} = \rho n_O[0{\cdot}315k_{f_1} n_{N_2} + 0{\cdot}132k_{f_2} n_{NO} + 0{\cdot}493k_{f_3} n_{O_2}] \times 10^3 \text{ MJ kg}^{-1}, \tag{15}$$

where n_O, n_{N_2}, n_{NO}, n_{O_2} are the molal concentrations of the reactants and k_{f_1}, k_{f_2}, k_{f_3} are the forward reaction rate constants of reactions (1), (2) and (3) respectively.

Following Hayes & Probstein (1959), boundary-layer similarity variables are defined as

$$\eta(x,y) = \frac{u_e}{\sqrt{2\xi}}\int \rho\, dy \quad \text{and} \quad \xi(x) = \rho_w . \mu_w . u_e x, \tag{16}$$

where y is the co-ordinate measured normal to the plate surface.

Along a streamline given by ψ = constant

$$d\psi = \frac{\partial\psi}{\partial x}\, dx + \frac{\partial\psi}{\partial\eta} . d\eta = 0, \tag{17}$$

where $\psi = \int_0^y \rho u\, dy$.

Using Equations (16) and (17)

$$x\frac{u}{u_e}\frac{d\eta}{dx} = -\tfrac{1}{2}\int_0^\eta \frac{u}{u_e}\, d\eta.$$

For an assumed linear velocity profile, given by $\eta = 2{\cdot}2u/u_e$, equation (15) for the energy absorption rate distribution across the boundary layer may be written as

$$\frac{d\epsilon}{d\eta} = -\frac{8{\cdot}8x}{u_e\eta^2}\rho n_O[0{\cdot}315k_{f_1}n_{N_2} + 0{\cdot}132k_{f_2}n_{NO} + 0{\cdot}493k_{f_3}n_{O_2}] \times 10^3 \text{ MJ kg}^{-1}.$$

This equation has been integrated across the boundary layer to find the total energy $\Delta\epsilon$ absorbed by the forward steps of reactions (1)–(3) at various stream-wise positions. In performing the integration, the reaction rate constants, k_f's, were evaluated at the local temperature T which is determined from

$$Cp\frac{dT}{d\eta} = \frac{dh}{d\eta} - \frac{d\epsilon}{d\eta}$$

and

$$\frac{dh}{d\eta} = \left(\frac{H_e - h_w}{u_e} - \eta\frac{u_e}{2{\cdot}2}\right)\frac{u_e}{2{\cdot}2}.$$

The effect of the energy $\Delta\epsilon$ absorbed by the endothermic reactions on the surface Stanton number was deduced by assuming that the maximum enthalpy within the boundary layer was reduced by the amount $\Delta\epsilon$ compared with the non-reacting case. A modified recovery enthalpy h_r'' was then calculated, by effecting a nominal reduction in the external flow velocity to match the reduced maximum enthalpy, and a modified Stanton number S'' was obtained and defined as

$$S'' = q_w/\rho_e u_e(h_r'' - h_w).$$

The results of calculations comparing the modified Stanton number S'' with that based on frozen, non-reacting boundary-layer behaviour and defined by

$$S_f = \dot{q}_w/\rho_e u_e((h_r)_f - h_w)$$

where $(h_r)_f$ is defined in equation (5), are given in table 4.

For most of the experimental conditions for the zero incidence flat plate, the reduction in the Stanton number caused by endothermic reactions involving oxygen atoms is less than 5% at the trailing edge of the flat plate. More significant reductions are observed for the higher density experimental conditions in the $M = 5$ contoured

	1·27 cm nozzle throat diameter					2·54 cm nozzle throat diameter			
Test condition	B	B	A	A	A^+	B_c	B_c	B_c^+	B_c^+
Stagnation pressure p_0 (bar)	270	270	250	250	260	206	206	410	410
Stagnation enthalpy h_0 (MJ kg^{-1})	21·9	21·9	38·2	38·2	51	16·6	16·6	17·0	17·0
Plate incidence	0°	12°	0°	12°	0°	0°	0°	0°	0°
Distance from leading edge x (m)	0·50	0·15	0·50	0·15	0·50	0·05	0·50	0·05	0·50
$\Delta\epsilon$ (MJ kg^{-1})	0·21	0·73	0·24	1·06	1·85	0·18	0·75	0·52	1·24
S''/S_f	0·95	0·84	0·97	0·85	0·92	0·95	0·79	0·86	0·66

TABLE 4. Effect of boundary-layer endothermic reactions on Stanton number

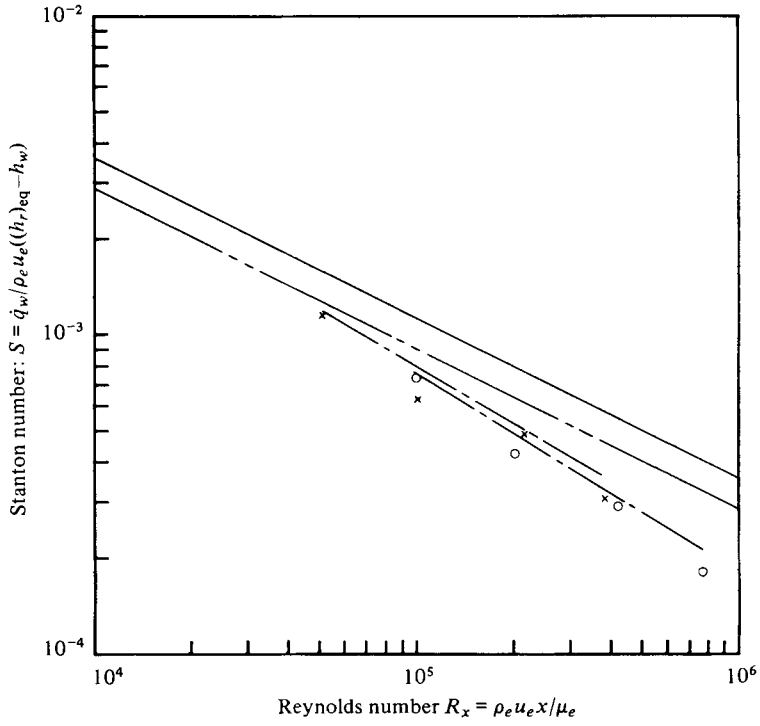

FIGURE 9. Stanton number versus Reynolds number data for a zero incidence flat plate in the contoured nozzle. ——, theory, fully catalytic plate; — - - —, theory, non-catalytic plate; — · — · —, theory, non-catalytic plate plus endothermic boundary-layer reactions. ○, experiment B_c^+, $h_0 = 17{\cdot}0$ MJ kg^{-1}, $p_0 = 430$ bar; ×, experiment B_c, $h_0 = 16{\cdot}6$ MJ kg^{-1}, $p_0 = 220$ bar.

nozzle experiments shown in figure 9. The simple approximate theory provides good agreement with both the observed magnitude and streamwise fall in heat transfer along the plate.

Boundary-layer reaction effects are also significant for the higher densities which occur with the plate at 12° incidence. Table 4 shows that the Stanton number is reduced by approximately 15% compared with the non-catalytic wall, frozen boundary-layer value. The inclusion of boundary-layer reactions, therefore, improves the

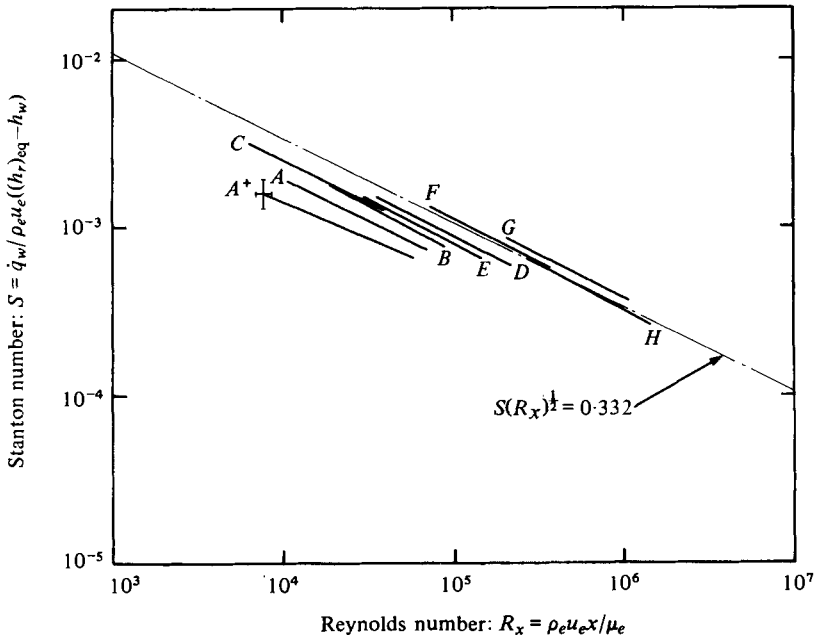

FIGURE 10. Stanton number versus Reynolds number data for a zero incidence flat plate. ——, mean line through experimental data for 1·27 cm nozzle throat diameter. Run types A^+ to H defined in table 1. ⊢⊣, indicates typical error margin (maximum) for run type A^+ (worst case).

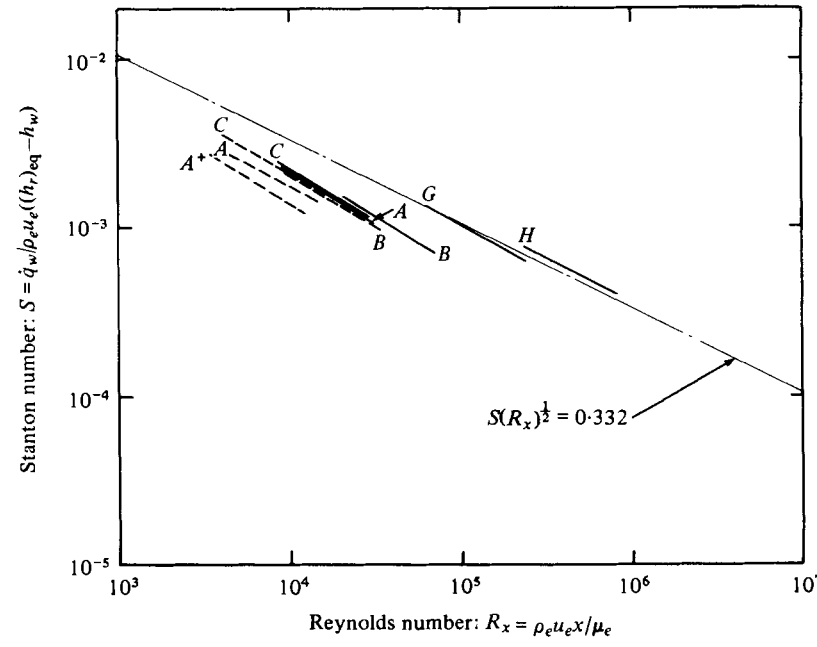

FIGURE 11. Stanton number versus Reynolds number data for a 12° incidence flat plate. ——, mean line through experimental data for 1·27 cm nozzle throat diameter. – – –, mean line through experimental data for 0·635 cm nozzle throat diameter. Run types A^+ to H defined in tables 2(*a*) and 2(*b*).

agreement between experiment and theory shown in figure 11 for the higher density 1·27 cm nozzle throat condition, but the effect for the lower density 0·635 cm nozzle throat experiments is insignificant. It is possible that the observed differences for the lower-density experiments may be due to the vibrational excitation of N_2 by the oxygen atoms within the boundary layer. Breshears & Bird's (1968) rate data for the vibrational process

$$N_2 + O \rightarrow N_2^* + O$$

shows that vibrational equilibrium is marginal for the 0·635 cm throat experiments. If vibrational de-excitation rates are lower than the excitation rates at the conditions prevailing in the boundary layer, then vibrational excitation of the nitrogen molecules could account for sufficient energy to explain the observed lower surface heat transfer rates for these cases.

7. Discussion of results

Figure 10 shows the zero incidence dimensionless heat-transfer rate results compared with the simple Blasius laminar boundary layer result of $S(R_x)^{\frac{1}{2}} = 0{\cdot}332$ where S and R_x have been defined using equations (1) and (2). The agreement is better for the low enthalpy flow conditions (H, F, G) where the test section flow is undissociated and behaves as a perfect gas. As the magnitude of the enthalpy associated with the frozen test section composition increases, the predictions of simple theory over predict the Stanton number based on h_r (eqn. 4) by up to 100% for run condition A^+. Similar trends are observed for the 12° incidence plate results shown in figure 11.

The predictions of the simple theory do not take into account the variation in the viscosity–density product across the boundary layer and more accurate estimates of the S–R_x relationship, based on the intermediate enthalpy method using equation (12), have been made for each of the individual run conditions. These are given in tables 1 and 2. Figures 12 and 13 show the experimental Stanton numbers at a given streamwise station ($x = 5{\cdot}7$ cm for 0° and $x = 4{\cdot}4$ cm for 12°) compared with the predictions of the intermediate enthalpy method. Increasing departure between theory, assuming equilibrium flow ($k_w = \infty$), and experiment is apparent as test section velocity increases. However, if the Stanton number is redefined and based on the frozen recovery enthalpy $(h_r)_f$ only, much better agreement with experiment is observed. This limit corresponds to frozen gas phase reaction ($\zeta_g \rightarrow 0$) and frozen surface reactions ($E(x, \sigma) \rightarrow 1$ or $k_w \rightarrow 0$). A similar trend is observed for both 0° and 12° plate results.

Exceptions to the generally satisfactory level of agreement are for run conditions in excess of 25 MJ kg^{-1} stagnation enthalpy. The estimated level of the frozen enthalpy fraction fails to account for the low Stanton numbers observed. A possible explanation is the presence of helium in the test gas for these conditions. The nozzle and plate flow starting times given in figure 5 preclude measurements before 450 μs, by which time Crane (1975) has shown that the helium contamination level is about 40%. Estimates of the $S \sim R_x$ relationship for such assumed test section compositions show that the $S(R_x)^{\frac{1}{2}}$ product falls when the helium arrives owing to the increase in Reynolds number associated with the cooler helium. Figure 5 suggests that run conditions A and A^+ will be affected to some extent by this phenomenon but that for all other conditions the results can be taken to be helium free.

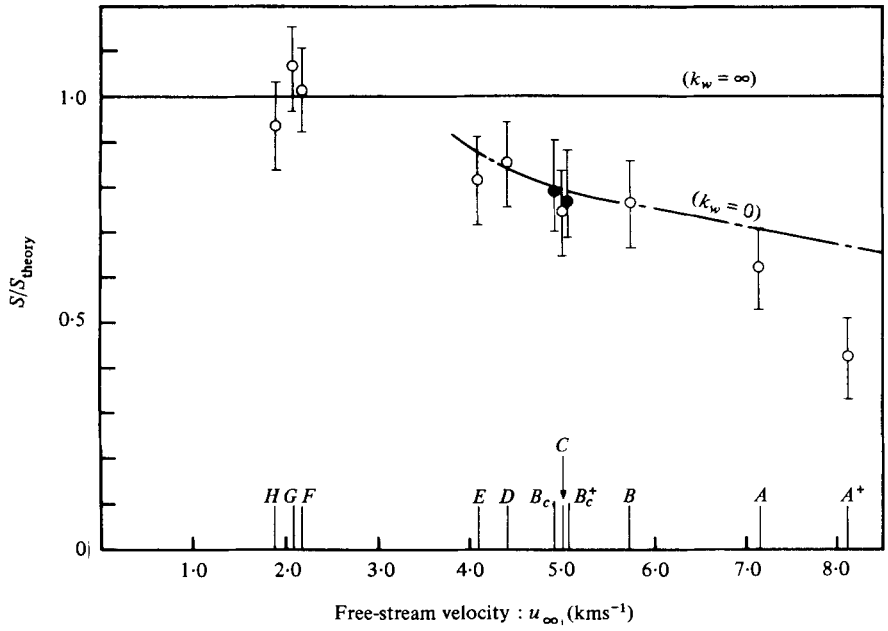

FIGURE 12. Comparison of heat transfer measurements at $x = 5{\cdot}7$ cm with intermediate enthalpy theory (0° incidence). ——, theory, fully catalytic surface; — · —, theory, non-catalytic surface. ⊖, experiment, 1·27 cm nozzle throat diameter; ⊖, experiment, 2·54 cm nozzle throat diameter (corrected for boundary layer endothermic reactions). Run types A^+ to H defined in table 1.

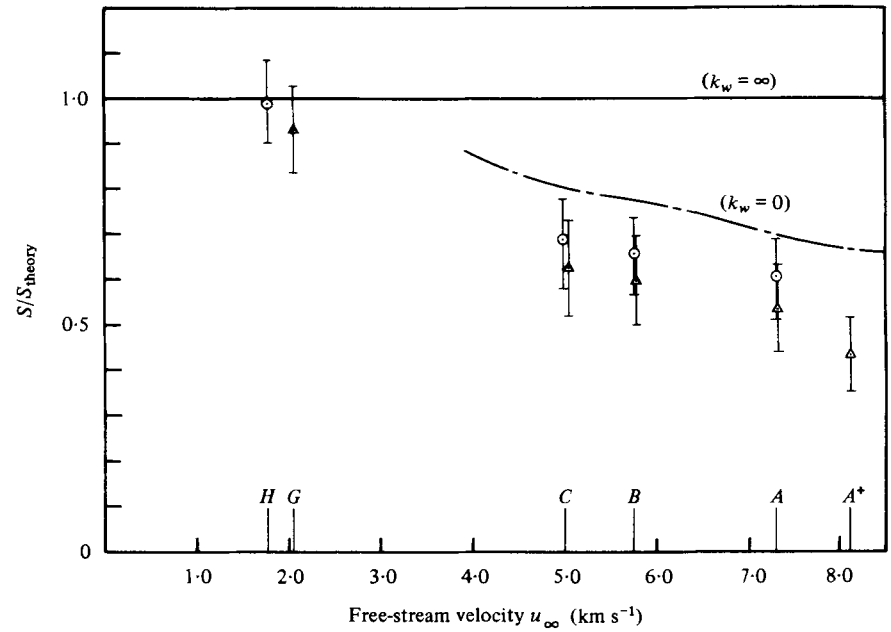

FIGURE 13. Comparison of heat transfer measurements at $x = 4{\cdot}4$ cm with intermediate enthalpy theory (12° incidence). ——, theory, fully catalytic surface; — · —, theory, non-catalytic surface. ⊖, experiment, 1·27 cm nozzle throat diameter; ⊖, experiment, 0·635 cm nozzle throat diameter. Run types A^+ to H defined in tables 2(*a*) and 2(*b*).

Some additional confirmation of this effect was obtained by East, Stalker & Baird (1977) by purposely filling the shock tube with equal parts (by pressure) of air and helium to result in similar shock speeds (and hence stagnation enthalpy) to the pure air cases.

With the exception of the helium contaminated flows, the experiments in the conical nozzle flow give best agreement with predictions based on chemically frozen flow, both in the gas phase within the boundary layer and at the surface. These conclusions are consistent with the estimates of the gas phase and surface reaction Damkohler numbers which are summarized in table 3 and suggest that all of the experimental conditions tested were close to the frozen flow limit. For the 12° incidence case, the experimental results appear to be somewhat lower than the frozen-boundary-layer predictions but here it is postulated that the enthalpy absorbed by endothermic boundary layer reactions discussed earlier may account for this. An additional uncertainty is the test gas viscosity at the high temperature non-equilibrium free-stream condition.

For the 0° plate, the maximum flow temperature at which the viscosity was evaluated was $\sim$ 1500 K whereas for the 12° plate the corresponding value was $\sim$ 3500 K. The known frozen composition of the test gas is quite different from the assumed equilibrium composition on which the viscosity estimates have been based. Further work on the estimation of viscosity for non-equilibrium mixtures with high concentrations of atomic species is evidently required.

For the contoured nozzle experiments at high free-stream density and at Mach number 5, an important additional trend of a stream-wise reduction of Stanton number greater than the predicted $R_x^{-\frac{1}{2}}$ rate is shown in figure 9. Surprisingly good agreement was noted with an approximate model which considered the possibility of endothermic reactions in the boundary layer involving oxygen atoms described earlier. Further refinement is required, but it appears probable that this mechanism can account for the observed surface heat-transfer rates which are lower than even the non-catalytic surface, frozen gas-phase limit.

9. Conclusions

For the higher-Mach-number, lower-density experiments heat-transfer measurements compare well with the predictions of an intermediate enthalpy method for the compressible laminar boundary layer at flow stagnation enthalpies up to about 25 MJ kg^{-1}, corresponding to flow velocities up to about 6 km s^{-1}. All conditions explored resulted in apparently frozen gas phase and surface recombination reactions. These conclusions were consistent with predictions of the appropriate Damkohler criteria based on the oxidized metal (aluminium) surface of the 0° plate and the SiO_2 coated surface of the 12° plate. It would appear unlikely that significant amounts of the frozen chemical enthalpy would be recovered unless pure unoxidized metal surfaces are used. Departures from the predictions of the intermediate enthalpy theory may be accounted for either by helium contamination of the test section flow at highest enthalpies or by uncertainty in the viscosity at the high static temperatures on the 12° plate.

A further possible factor affecting the surface heat-transfer measurements is that of endothermic gas phase reactions in the boundary layer involving the large oxygen-

atom concentrations and resulting in the formation of NO and N. These effects are important at higher densities and the predictions of an approximate model suggest that the large observed streamwise reduction of heat transfer in higher density, lower-Mach-number experiments performed in a contoured nozzle may result from this. Similar, but smaller effects, may account for some of the differences between experiment and frozen flow theory at the relatively high density on the 12° incidence plate positioned in the conical nozzle.

The authors acknowledge the generous assistance of Mr R. French and the technical staff of the Physics Department, Australian National University (A.N.U.) with the experiments in the T3 shock tunnel. Thanks are also expressed to Dr B. J. McCaffrey and Mr M. W. Stent of the University of Southampton and Mr S. Furler of A.N.U. for their expertise in the manufacture of the heat-transfer sensors and associated calibration and recording equipment. Generous financial assistance was provided by the School of General Studies, A.N.U. and by the Procurement Executive, Ministry of Defence, which enabled one of the authors (R.A.E.) to visit the Australian National University to participate in the experimental programme.

The construction and development of the free piston shock tunnel T3 was supported by the Australian Research Grants Committee.

REFERENCES

Bauer, E. & Zlotnick, M. 1959 Transport coefficients of air to 8000 K. *ARS J.* **29**, 721–728.

Bray, K. N. C. 1970 Non-equilibrium flow problems of space shuttles. *Aero. Res. Counc. Rep.* 32, 408.

Breshears, W. D. & Bird, P. F. 1968 *J. Chem. Phys.* **48**, 4678–4683.

Chung, P. M. 1965 Chemically reacting non-equilibrium boundary layers. *Advances in Heat Transfer*, vol. II, pp. 109–270. Academic.

Crane, K. C. A. 1975 Mass spectrometry in pulsed hypersonic flows. Ph.D. thesis, Australian National University.

Davies, L. & Wilson, J. L. 1969 Influence of reflected shock and boundary layer interaction on shock tube flows. *Phys. Fluids Suppl.* **12**, I 37–43.

Davies, W. R. & Bernstein, L. 1969 Heat transfer and transition to turbulence in the shock-induced boundary layer on a semi-infinite flat plate. *J. Fluid Mech.* **36**, 87–112.

Dorrance, W. H. 1962 *Viscous hypersonic flow.* McGraw-Hill.

East, R. A., Stalker, R. J. & Baird, J. P. 1977 Laminar flat plate heat transfer measurements from a dissociated high enthalpy hypersonic airflow. *Univ. of Southampton, Rep.* AASU 338.

Hayes, W. D. & Probstein, R. F. 1959 *Hypersonic Flow Theory.* Academic Press.

Hirschfelder, J. O., Curtis, C. F. & Bird, R. B. 1954 *Molecular Theory of Gases and Liquids.* John Wiley.

Lordi, J. A., Mates, R. E. & Moselle, J. R. 1966 Computer program for the numerical solution of non-equilibrium expansion of reacting gas mixtures. *N.A.S.A. Rep.* NASA CR-472.

Lordi, J. A., Vidal, R. J. & Johnson, C. B. 1971 Chemical non-equilibrium effects on the flow in the windward plane of symmetry of a blunted delta orbiter. *N.A.S.A. Rep.* TMX 2508.

McCaffrey, B. J., East, R. A. & Stent, M. W. 1975 A thin film catalytic-non–catalytic heat transfer gauge for shock tube measurements in reacting gases. *Univ. of Southampton, Rep.* AASU 336.

Rosner, D. E. 1963 Scale effects and correlation in non-equilibrium convective heat transfer. *A.I.A.A. J.* **1**, 1550–1555.

Schultz, D. L. & Jones, T. V. 1973 Heat transfer measurements in short-duration hypersonic facilities. *AGARDograph* 165.

SMITH, C. E. 1966 The starting process in a hypersonic nozzle. *J. Fluid Mech.* **24**, 625-640.

STALKER, R. J. 1972 Development of a hypervelocity wind tunnel. *J. Roy. Aero. Soc.* **76**, 374–384.

STALKER, R. J. & CRANE, K. C. A. 1978 Driver gas contamination in a high enthalpy reflected shock tunnel. *A.I.A.A. J.* **16**, 277–279.

STALKER, R. J. & MCINTOSH, M. K. 1973 Hypersonic nozzle flow of air with high initial dissociation levels. *J. Fluid Mech.* **58**, 749–761.

STALKER, R. J. & STOLLERY, J. L. 1975 The use of a Stalker tube for studying the high enthalpy non-equilibrium air flow over delta wings. In *Modern Developments in Shock Tube Research*. Japan: Shock Tube Research Society.

VIDAL, R. J. & GOLIAN, T. C. 1967 Heat transfer measurements with a catalytic flat plate in dissociated oxygen. *A.I.A.A. J.* **5**, 1579–1588.